Fundamental Superconducting Effects in Lead, Vanadium, and Niobium.

Samuel James Bader
MIT Department of Physics
(Dated: May 4, 2013)

This paper reports the results from three experiments of fundamental superconducting phenomena. First, transition temperatures are found for vanadium, lead, and niobium using the Meissner effect, and, although the temperatures determined reveal a systematic bias in the apparatus, the Meissner effect is clearly seen. Second, flux trapping is demonstrated in a superconducting cylinder, and results clearly show a trapped magnetic field within experimental precision. Finally, the I-V characteristics of a Josephson junction are used to determine the niobium superconducting gap, and find the value of the magnetic flux quantum within one sigma of the accepted value.

I. INTRODUCTION

Superconductitivity, the resistanceless flow of current and perfect expulsion of magnetic fields, is a beautiful example of quantum behaviour manifested on a macroscopic system. In the century since its discovery, superconductivity has seen application in a wide range of practices, from magnets for medical imaging to potential qubits for quantum computing, even while many fundamental physical questions remain unanswered [3]

This experiment surveys several of the fundamental phenomena in superconductivity: using the Meissner effect to find transition temperatures, trapping magnetic flux inside a superconducting cylinder to produce an extremely stable magnet, and probing the current-voltage characteristics of Josephson junctions to determine the value of the magnetic flux quantum.

II. APPARATUS

The three experiments discussed herein made use of three separate probes. The features of each probe are discussed within each relevant section (III, IV, V), and the overall matters of procedure are addressed here.

For each experiment, a probe is fasted in the neck of a large dewar holding typically $\sim$ 25L of liquid He provided by the MIT Cryogenic Lab. The head of the probe sits near the base of the dewar neck (for the T_c probe, this is 10cm above the base, and for the flux-trapping probe, this is 4cm above the base, whereas for the Josephson probe, this height is adjusted to set the temperature.)

Control over temperature is a difficulty in this experiment. The two probes whose positions are fixed allow temperature control by pumping helium out of the dewar through the probe and varying the flow rate. Temperature is measured from the voltage across a calibrated silicon diode (or carbon resistor for the flux-trapping probe), but this is a major source of uncertainty. First, the current source which supplies the diode current experiences fluctuations which, at the most sensitive points of the calibration, may affect the temperature readout by about $\sim$.1K. Second, the temperature gradient along the probe is large and non-uniform (and proper calculation would have to account for the effects of cold gas flow in addition to the heat conduction). For a rough estimate, the temperature needs to increase 270K over about 50cm, so it is not difficult to imagine that a diode .5cm away could be off by a shift of up to 2.7K. These considerations will soon become important.

III. TRANSITION TEMPERATURES

The first part of the experiment uses the sudden, complete rejection of magnetic field by a superconductor in order to locate the transition temperatures of vanadium, niobium, and lead.

The probehead for this experiment contains two coils: the outer solenoid (2200 turns, 31.0mm) and the inner "test" coil (810 turns, 12.0mm), wrapped around an interchangeable superconducting cylinder. An AC voltage of $500\text{mV}_{\text{rms}}$[1] at 200Hz is applied to the solenoid to generate an AC magnetic field, which couples into the inner test coil to produce a produce an AC voltage in the test coil on the order of 3mV.

Above their critical temperatures, all the superconducting materials have negligible magnetic properties and don't interfere with the inductive coupling of the coils. However, below their critical temperatures, the superconductors perfectly oppose the fields of the outer coil within their bulk, thus reducing the signal from the test coil. This change in the test coil signal, which in our experiment amounts to typically a $\sim$20% (or $\sim$.7mV) change over the span of about .5 Kelvin, marks the transition temperature.

Figure 1 shows several scans of the transition in vanadium, which displays some hysteretic behavior. Each scan is fit to a logistic curve and the center temperatures are averaged together to produce a final T_c estimate. The variation in that averaged set is taken as a statistical uncertainty, and the thermometer uncertainty

[1] Note that $500\text{mV}_{\text{rms}}$ is merely the nominal setting on the Agilent function generator; the actual voltage supplied to the test coil is measured to be on the order of $100\text{mV}_{\text{rms}}$ because the generator is loaded down by the low-impedance coil.

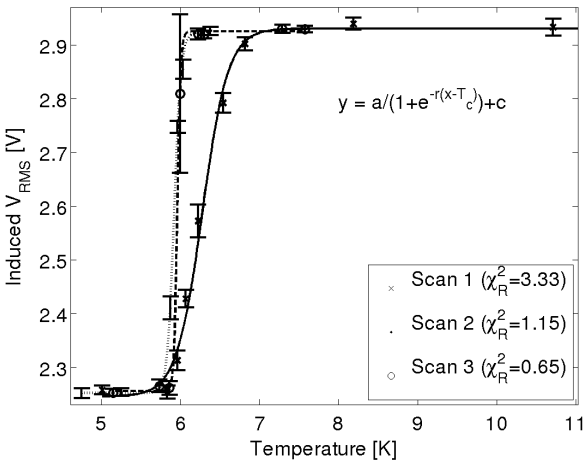

FIG. 1: Transition curves for the Vanadium sample showing $T_c = 6.05 \pm .11_{\text{stat}} \pm .08_{\text{sys}}$K, statistical errors coming from the fitting uncertainties, systematics coming from the hysteretic variation.

given by current variations (discussed in Sec. II, but computed for each temperature separately from the calibration curve) gives the systematic error. Each of these data should also be taken with the understanding that an overall shift from the temperature gradient (as also discussed in Sec. II) may apply.

The transition temperatures for each sample are shown in Table I. The transition in niobium, like that in vanadium, is sharp and well-defined, whereas the transition in lead is complicated by broader temperature dependent behaviour, producing a wide, dominant systematic uncertainty. These temperatures are generally a couple of Kelvin above the accepted values, most likely due to temperature gradient between the temperature diode and the sample.

Sample	T_c	σ_{stat}	σ_{sys}	Accepted
V	6.05	.01	.08	5.40
Pb	9.50		3.91	7.20
Nb	12.72	.07	.13	9.25

TABLE I: Fitted transition temperatures and uncertainties for each sample, compared with previously accepted values (all in Kelvin). Note that time constraints limited the number of measurements on Pb, which is why no statistical uncertainty is given.

For the purposes of this paper, the transition temperature determination serves more as a background for the demonstration of the exciting effects to be discussed in the coming sections, but more information on this topic can be found in the companion paper by Zhou.

IV. PERSISTENT CURRENTS

As discussed previously, a key distinction of the superconductor is its perfect diamagnetism, its ability to expel all magnetic field lines from the material bulk. Since magnetic field lines cannot pass through the material once superconducting, a hollow circle or cylinder of superconducting material can be used to trap field lines inside.

The probe for this experiment contains a hollow lead cylinder (9cm long, with inner diameter 1.11cm, outer diameter 1.43cm). A 2210 turn, 4.45cm solenoid is wound about the cylinder, and a Hall probe and carbon resistor thermometer are both inside.

A field is passed through the cylinder when above the critical temperature, and then the cylinder is cooled into the superconducting phase, at which point the superconducting body will expel magnetic field, but the hollow core will not. The lines passing though the core, topologically speaking, are trapped by the perfect diamagnetism surrounding them. Even if the external source of magnetic field is removed, the magnetic field passing through the core must not change, and supercurrents will flow within the cylinder in order to guarantee just this.

This can be seen in Figure 2, which contains four scans of the solenoid current. One scan is taken above the critical temperature to demonstrate that the Hall probe gives a voltage linear in magnetic field ($\chi^2_R = .55$). Then, three separate times, the solenoid current is set to some value (0mA, 50mA, 100mA), the sample is cooled down, and the solenoid current is scanned from 0mA to 100mA to demonstrate that the Hall voltage does not change (within the discretization uncertainty) once the sample is superconducting. This perfectly fixed (within discretization error) magnetic field measurements powerfully demonstrates the phenomenon of "frozen-in flux" protected by supercurrents.

V. JOSEPHSON JUNCTIONS

Whereas the previous experiments have focused on the characteristics of a single body of superconducting material at a time, further effects can be observed by coupling together multiple superconducting regions. A Josephson junction is precisely that situation: two blocks of superconductor with a thin insulating layer between to allow for tunnelling. Certainly, should the voltage across the junction be high enough, electrons may break out of the Cooper pairs and tunnel across the insulating layer. Brian Josephson's Nobel-winning prediction was that Cooper pairs themselves could also tunnel through the junction, with a rather remarkable I-V characteristic [3].

The probe for this experiment uses one junction on a chip of 81 circular niobium/ aluminum oxide/ niobium Josephson junctions, each wired for a four-point resistance measurement. Each junction is 15μm in diame-

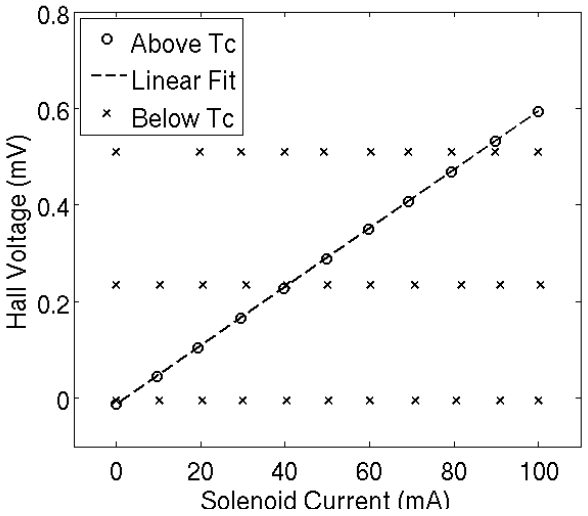

FIG. 2: Demonstration of persistent supercurrents. Circles represent data taken above T_c, where the magnetic field (given by the Hall voltage) is just linear in the solenoid current. The crosses represent data taken below T_c, where the superconducting cylinder prevents any change in the magnetic field. Note: individual error bars, which arise from discretization error in measurement, are too small to appear.

ter, with an oxide thickness of 1.75±.25nm. The voltage across a nearby silicon diode provides a temperature reading.

Feynman [1] gives a brief and accessible derivation of the electrical characteristics which will be observed in this section. Since some parts of the later analysis depend on the principles of the Josephson junction, this derivation is summarized below.

V.1. IV Characteristic

For a junction as depicted in Figure 3, consider the Cooper pair wavefunction as having two components: ψ_1 on the left side of the junction, and ψ_2 on the right. A voltage V is applied across the junction to create a difference in the energy levels, and some non-zero tunnelling element K is assumed, leading to the usual two-state equations:

$$\dot{\psi_1} = \frac{qV}{2}\psi_1 + K\psi_2, \quad \dot{\psi_2} = -\frac{qV}{2}\psi_2 + K\psi_1$$

One may then interpret the component $\psi_i = \sqrt{\rho_i}e^{i\theta_i}$ in terms of the probability ρ_i of finding a Cooper pair in side i; this is useful because, in a macroscopic ensemble of Cooper pairs, the carrier density in side i is proportional to ρ_i. With this interpretation, the current across the junction is then proportional to $-\dot{\rho}_1 = \dot{\rho}_2$. Additionally, any physical quantity having to do with the phases θ_i should be expressible in terms of $\delta = \theta_1 - \theta_2$, since the global phase is unobservable.

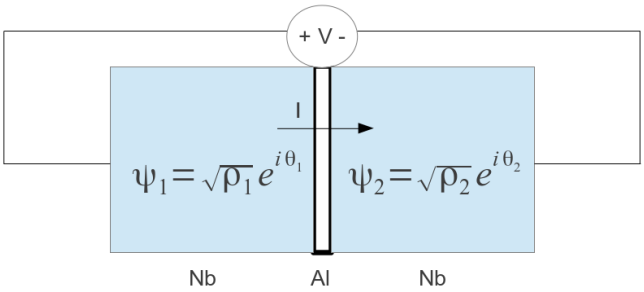

FIG. 3: Two-state model for deriving the Josephson equations, where the amplitude in each state is written explicitly in terms of the probability ρ_i to find the Cooper pair in this state.

Substituting in this interpretation and solving will then give the current-voltage relation across the junction. Of course, in practice, the ρ_i should not be changing at all, since any Cooper pair which tunnels across the junction must be replenished by the circuit; nonetheless, this intuitive method yields the correct relations, known as the Josephson equations [1]:

$$J = J_0 \sin\delta, \quad \delta = \delta(0) + \frac{2e}{h}\int_0^t V dt$$

where the constant J_0 absorbs the geometry of the junction, thickness of the insulating layer, etc.

V.2. Results

Consider these relations in more depth. At $V = 0$, δ is any constant, so any current (with magnitude less than J_0) may flow through the junction at zero-voltage. This is evident in the center of the experimental I-V curve of Figure 4. At finite voltage, δ oscillates with angular frequency $2eV/h$. Since $2e/h = 484\text{MHz}/\mu\text{A}$, even the smallest voltages will produce current oscillations which average to zero faster than the timescale of standard equipment; thus there is effectively no current beyond 0V. That is, until the voltage reaches $2\Delta/e$, and provides the energy necessary to break a Cooper pair, and we begin to see an ohmic current due to electron tunnelling [3], visible on either side of the scope trace.

From the IV curve in Figure 4, we easily determine the superconducting gap in niobium. The start of each normal-conducting line should be $2\Delta/e$ from the 0V point, so, setting the cursors at the onset of normal conduction, we take the cursor voltage difference, divide out a factor of four and the 100x amplification, and read off $\Delta = .70 \pm .12\text{meV}$, where the systematic uncertainty comes from the width of the 200Hz oscilloscope trace.)

For comparison, Novotny and Meincke [4] extrapolate a zero-temperature niobium gap of $\Delta(0K) = 1.45\text{meV}$

(and a $T_c = 9.26$). Townsend and Sutton [2] report that the temperature dependence of the energy gap obeys

$$\frac{\Delta(T)}{\Delta(0K)} = \tanh\left(\frac{\Delta(T)}{\Delta(0)} \times \frac{T_c}{T}\right)$$

Solving this, we find that our Δ is consistent with a temperature of $.92T_c$, or $8.5K$, which is about 5% lower than our nominal temperature of 8.9K. This will be useful in estimating our probe-specific temperature uncertainties in the flux quantum analysis.

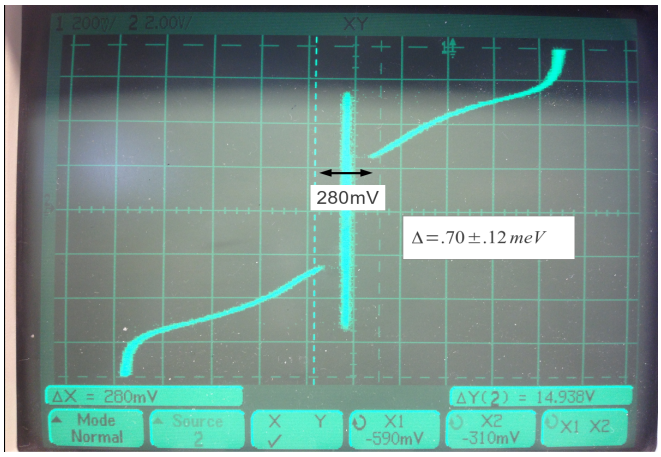

FIG. 4: Oscilloscope trace demonstrating the Josephson IV relations at a nominal temperature of 8.9K. (Vertical axis is uncalibrated current, horizontal axis is the junction voltage amplified by a factor of 100). This trace shows a niobium superconducting energy gap of $\Delta(8.9K) = .70 \pm .12$meV.

V.3. Magnetic field dependence

The application of a magnetic field through the insulating region parallel to the plane of the junction also produces an interesting modulation of the current, from which the magnetic flux quantum can be determined.

A magnetic field B through the junction (of side-length L and thickness t) can be accounted for by a vector potential A of magnitude $Lt_{\text{eff}}B/2$ on both sides (where the t_{eff} takes into account field penetration into the superconducting regions, and will be discussed shortly). Referencing Equation 1 for the current density, we see that, in order that there be no current parallel to the junction, the phase must vary along the junction.

$$J = \frac{\hbar}{m}(\nabla\theta - \frac{q}{\hbar}A) \tag{1}$$

The effect of this variation is a position (x) dependence of $\delta(x) = \delta_0 + qLt_{\text{eff}}Bx/\hbar$ along the junction perpendicular to the field. Since the current density $J(x)$ is a function of $\delta(x)$, the current density varies with position, and the total current can be found by integrating $J(x)$ over x. The maximal current which one would measure at a specific value of the magnetic field can be found by maximizing $\int J dx$ over the possible values of δ_0. One finds

$$J_0 \propto \max_{\delta_0} \int_0^L dx \sin\delta(x) \propto \text{sinc}(B/B_0)$$

where B_0 is such that $B_0 L(2\lambda{+}t) = h/2e$. Figure 5 shows intuitively how this will modulate the current, resulting in a $\text{sinc}(B/B_0)$ dependence for a rectangular junction [5].

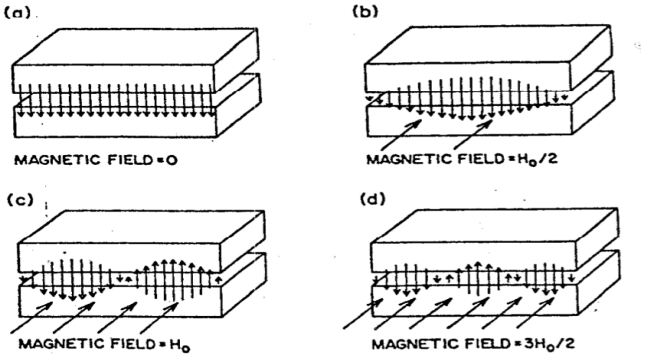

FIG. 5: Magnetic field varies the phase along the junction, modulating the current. Reprinted from [5].

Measurements of the current modulation by magnetic field are shown in Figure 6, along with three fits. The above mentioned standard sinc functional form is named the "rectangular" fit. However, we see that it does not fall off quite as fast as the data at high field. One cause for this deviation is that our junctions are not actually rectangular, but circular. To account for this, we model the junction as a sum of many infinitesimal rectangular junctions of length l, and integrate these contributions together, each weighted by a factor of l (since each junction contributes a current proportional to its length) and a Jacobian factor of $l/\sqrt{l^2 + L^2}$ from the circular shape. Then the total is maximized over δ_0 (this maximization should be done with the overall expression rather than for each slice, since the phases of the junction slices are tied together). The result is non-analytic; the final expression used for fitting is as follows:

$$J_0 \propto \max_{\delta_0} \int_0^L dl \frac{l^2}{\sqrt{(l/2)^2 + (L/2)^2}} \frac{B_0}{B} \times \left\{\cos(2\pi \frac{Bl}{B_0 L} + \delta_0) - \cos(\delta_0)\right\} \tag{2}$$

Equation 2 is used for the "circular" fit, which, as we see in Figure 6, captures more but not all of the high-field fall-off. Finally, the "suppressed" fit simply multiplies that standard sinc dependence by an unmotivated exponential factor to force it down to the high field data. χ^2_R values and B_0 values are given for each fit in Table II.

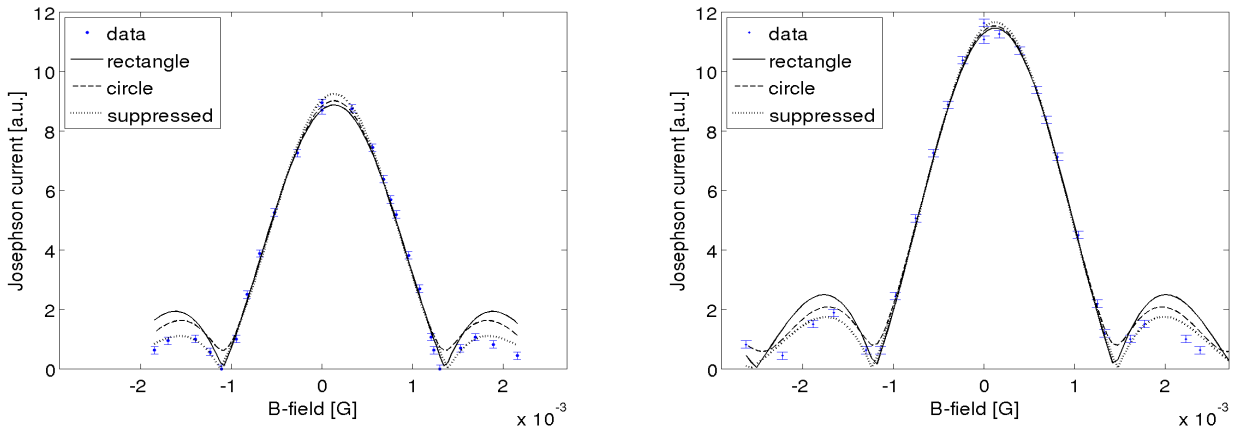

FIG. 6: Variation of the Josephson current with magnetic field at nominal temperatures of 8.2K (left) and 7.1K (right). Three fits are shown to the data points. The "rectangle" fit (solid) uses the standard $\mathrm{sinc}(B/B_0)$ expression. The "circle" fit (dashed) modifies the standard expression for a circular junction, and we see that it comes closer to the low-lying data points at high field. The "suppressed" fit simply multiplies the $\mathrm{sinc}(B/B_0)$ function by an (theoretically unjustified) $\exp(B/B_1)^2$ suppressing it to fit the low-lying data points.

	8.2K			7.1K		
	χ^2_R	B_0 [G]	σ_B [G]	χ^2_R	B_0 [G]	σ_B [G]
Rectangular	17.2	12.3	.2	15.7	13.2	.2
Circular	12.0	11.1	.2	6.6	12.1	.1
Suppressed	4.6	12.6	.2	6.8	13.5	.2

TABLE II: Fit values with statistical uncertainties for the data in Figure 6.

To find the flux quantum, we multiply the fitted magnetic field period B_0 by the dimensions of the junction $\Phi = B_0 L t_{\mathrm{eff}}$. The diameter, L, is simply 15µm, but the penetration-aware thickness, t_{eff}, includes a temperature dependence.

$$t_{\mathrm{eff}} = t + 2\lambda = 1.75\mathrm{nm} + 2 \times 39\mathrm{nm}/\sqrt{1-(T/T_c)^4}$$

This factor comes with a .25nm uncertainty in the actual junction thickness, as well as a propagated 5% temperature uncertainty, estimated earlier from the energy gap considerations. The B_0 values are averaged (within each temperature) from Table II, and the variation is used to estimate a systematic B_0 uncertainty from the procedure. Each average B_0 is multiplied by the respective dimensional factors, accounting for their various uncertainties.

The 8.2K run finds $\Phi = 1.90 \pm .13_{\mathrm{sys}} \pm .02_{\mathrm{stat}}$, and the 7.1K run finds $\Phi = 2.29 \pm .28_{\mathrm{sys}} \pm .03_{\mathrm{stat}}$. Averaging these two estimates together and estimating the systematic uncertainty by their difference, one finds

$$\Phi = (2.10 \pm .19_{sys} \pm .03_{stat}) \times 10^{-15}\mathrm{Wb}$$

which is within one sigma of the accepted value, $2.07{\times}10^{-15}$Wb.

VI. CONCLUSION

We have performed three fundamental experiments in superconductivity. In the process, we observed the Meissner effect in three materials, and used it to estimate the their transition temperatures, but were limited by large temperature uncertainties. We then moved on and observed a trapped flux in a superconducting cylinder. And finally, we used a Josephson junction to find the value of the magnetic flux quantum within one sigma of the known value.

[1] Feynman Lectures on Physics, Vol 3, Ch 31.
[2] Townsend and Sutton. Phys. Rev. 128, 2 (1962), 591-595.
[3] MIT Junior Lab Superconductivity Lab Guide.
[4] Novotny and Meincke. Journal of Low Temperature Physics, Vol. 18, Nos. 1/2, 1975.
[5] Scalapino, D.J., "Josephson Effects" in Encyclopedia of Physics, Edited by Lerner and Trigg, pp. 479-481